RESEARCH

Check for
updates

Effect of material characteristics of lead rubber isolators on seismic performance of box girder bridge

Mirza Aamir Baig[1*] , Imteyaz Ansari[1] and Nazrul Islam[1]

*Correspondence:
aamirmirzagarri@gmail.com

[1] Department of Civil
Engineering, Jamia Millia Islamia
University, New Delhi 110025,
India

Abstract

Near-field (NF) earthquakes have distinct ground motions, forward directivity pulses, and fling-step motions, causing structural responses to differ from far-field (FF) earthquakes. Seismic isolation is regarded as a developed and successful technology that may be applied to enhance a structure's functionality and safeguard it against catastrophic earthquake effects. The variation in mechanical properties of seismic isolation also significantly influences bridge seismic response. The study investigates the influence of lead rubber (LRB) isolators and the characteristics of ground motions on seismically isolated bridges, aiming to determine optimal parameters for minimal earthquake response. Key parameters include ground motion characteristics, characteristic strength (Q), and isolator flexibility. The study modeled the force-deformation behavior of isolators using bilinear behavior, reflecting the Bouc-Wen hysteric model. CSI Bridge was used to model seismically isolated steel box girder bridges, with eight natural accelerograms assessing a 2% probability of exceedance in 50 years. The peak responses of pier displacement (MPD), isolator hysteric energy (HED), base shear, and deck acceleration are chosen as the response parameters for the comparison. To evaluate the response parameters, the earthquake data are scaled to the three studied peak ground acceleration (PGA) levels of design level (0.2 g), extreme level (0.4 g), and rare-extreme level (0.8 g). The findings offer insight on the relevance of isolator stiffness and its influences on the seismic performance of isolated bridges. The study identifies minimum values for pier displacement, hysteric energy, deck acceleration, and base shear at specific Q/weight sustained by isolator (W) and time period (T) values. Recommendations are made for the preliminary seismic isolation design of bridges with LRB isolators, highlighting the importance of PGV to PGA ratio in earthquake damage assessment.

Keywords: Lead rubber isolators, Hysteric energy, Forward directivity, Steel box girder, Time history analysis

Introduction

India faces significant challenges in dealing with natural disasters and protecting life and property. With an average earthquake causing significant life and financial losses every 5 years, India is among the countries with high life losses. The Bhuj earthquake in 2001

Baig *et al. Journal of Engineering and Applied Science* (2024) 71:115

Page 2 of 19

prompted increased attention to disaster mitigation and management for seismic events. Reliable assessment of structures' seismic performance is crucial to preparing the country for minimizing the effects of seismic events, including structural damage, property loss, and life [22]. Seismic isolation applications, particularly in high seismicity developed countries, immediately reduce structural impact and shield nonstructural elements from harm after an earthquake.

Lead rubber bearing (LRB) and friction pendulum (FPS) systems are popular isolation systems for seismic protection of bridges, dissipating seismic energy through a hysteresis loop in the isolator's force deformation behavior. Rubber bearings, with their high-energy absorption capacity, are also widely used in seismically isolated projects worldwide. The bearing is composed of multilayered, laminated elastomeric material and has circular holes that hold lead plugs. It is rigid and stiff in the vertical direction, however flexible along the horizontal direction. Most seismically isolated bridges are analyzed and designed while considering design-level earthquakes in far fields, where the isolator experiences a nonlinear state while the superstructure remains linear, leading to concerns about isolator displacement and deck acceleration [7].

The behavior of isolated bridges during near-field earthquakes has gained significant interest due to the impulsive excitation exhibited by the structure. The response of bridge elements and isolators may differ significantly from far-field earthquakes, even at low levels of peak ground acceleration (PGA). More research is needed to examine the impact of different levels of PGA, the difference in response characteristics under forward directivity and fling-step actions of earthquakes, displacement demands and isolator nonlinearity, and the impact of pre- to post-yield stiffness on the behavior of seismically isolated bridges during near-field earthquakes.

The impacts of seismic isolators on bridge peak reactions, as well as the bidirectional interactions of isolation bearing for restoring the forces. The study compares the response of isolated bridges with non-isolated bridges, considering parameters like bridge pier flexibility, LRB stiffness, and yield strength. The findings reveals that the bidirectional interaction significantly impacts the bridge's seismic response [15]. Hassan and Billah [14] examine the impact of earthquake motion duration on the seismic behavior of bridges using two different isolators: a friction pendulum system and a lead rubber bearing. The significance of considering varying durations in seismic design is shown by the results, which demonstrate that long-duration vibrations can considerably impact the isolator and bridge response and cause more damage to bridge components. Asadi, Nikfar, and Hajirasouliha [2] utilize input factors such as rubber layers, radius, and material parameters to examine the effectiveness of LRB isolators. With various settings, 81 LRBs were used in a numerical experiment. The lead core radius was shown to have a substantial impact on LRB performance, but the number of rubber layers had minimal impact.

Shahbazi et al. [21] examine the impact of earthquake magnitude, duration, and intensity on the seismic performance of concrete bridges retrofitted with different isolation systems. The study used a box girder with rigid connections on cap beams and abutments, followed by isolators between the superstructure and substructure. Results showed that seismic retrofitting was correlated with seismic isolators, with FPS and LRB showing the best outcomes. The study also examined the effects of Landers and Loma

Baig *et al. Journal of Engineering and Applied Science* (2024) 71:115

Page 3 of 19

Prieta earthquakes, showing that earthquake magnitude and intensity significantly influence earthquake selection and response of bridges. The seismic vulnerability of a single circular cross-section pier on an Italian reinforced concrete (RC) bridge are considered for parametric study. The case study model is subjected to two analytical techniques: the response spectrum analysis (RSA) and the capacity spectrum method (CSM). The influence of geometrical and mechanical characteristics on the seismic vulnerability of the pier is evaluated by a parametric analysis. To evaluate the pier's seismic performance directly, the research suggests using a multilinear regression model [18].

The study uses a suggested optimum design technique to examine the seismic response of three distinct bridges with different isolation mechanisms and damping capacities. The bridges are examined with dominant seismic waves in the near and far field that are spectrum compatible. The findings suggest that, with an estimated overall damping ratio of 70%, the isolated bridge exhibits substantial damping, suggesting an excellent design decision when compared to other alternatives [17].

The study focuses on the optimal LRB design parameters for seismic isolation of bridges, highlighting the need for further research on the impact of LRB and earthquake characteristics on isolated bridge performance. The study evaluates the behavior of steel box girder bridges with LRBs as seismic isolation, examining the sensitivity of bridge response with variations in isolator design parameters. In order to determine the optimum LRB parameters for minimizing earthquake reactions in seismically isolated bridges, the study analyzes the performance of bridges isolated by LRB as well as the influence of PGA/PGV ratio as a damage indicator. The study uses numerical analysis to determine the most suitable seismic isolation parameter for LRBs by varying the characteristic strength to weight sustained by LRB isolators (Q/W). The numerical study employs nonlinear time history (NLTH) analysis to examine isolated bridges under seismic events, both near fault (NF) and far field (FF), and contrasts various response metrics, including pier displacement, base shear, isolator hysteric energy, and deck displacement. To evaluate the response parameters, the earthquake data are scaled to the three studied PGA levels of design level (0.2 g), extreme level (0.4 g), and rare-extreme level (0.8 g).

Near-field and far-field earthquakes

The majority of the fault energy in near-field earthquakes, which are usually directed within a 10–20 km radius, appears as pulses. Near-field (NF) earthquakes have higher acceleration and limited frequencies, with long-pulse periods in seismographs, contrasting with far-field earthquakes with higher frequencies. The maximal Fourier spectrum of these pulses often occurs within a narrow range of periods, while that of far-field earthquakes occurs over a wider range of times [1]. The fling-step and the forward directivity effect are two important factors that influence near-field earthquakes. The forward directivity effects develop when the fault rupture velocity is near the shear-wave velocity and the rupture direction is parallel to the site. This leads to damaging significant magnitude pulses with long periods and short durations [16]. Permanent ground displacement is an additional outcome of the geological deformations that lead to the fling-step effect, which results in large unidirectional amplitude velocity pulses and a monotonic step in the displacement accelerogram [28]. A substantial portion of the fault's energy is

Baig *et al. Journal of Engineering and Applied Science*   (2024) 71:115

Page 4 of 19

transmitted to the site with a large pulse at the initial phase of the seismogram when the fault propagates towards a location with a velocity near the shear-wave velocity. These effects are dependent upon the mechanism of rupture, the slip direction of the rupture with respect to the site, and the residual ground deformations, which are the three primary active parameters of NF earthquakes. In the fault-normal direction, forward-directivity pulses are directed close to the shear-wave velocity. Fling-step motions, which have a one-sided large-amplitude velocity pulse and a ramp-like step, are caused by static permanent ground displacements as a result of fault rupture [23]. Furthermore, for this mechanism, the fault waves eventually reach the structure in a progressive manner, but the fault waves are oriented in the opposite way which eventually travel farther apart and for longer periods of time. Near-field earthquakes' Fourier spectra reveal a spectrum that peaks within a limited wavelength and time period. The near-field structure design may be impacted by these pulse-like motions and an increase in seismic loads [26]. Figure 1 compares the NF (forward directivity), NF (fling step), and far-field earthquakes by analyzing their time histories. The presence of cyclic type waves in the far-field earthquake's time histories is evidently experienced. Long periods of pulses in the displacement, velocity, and acceleration time histories are characteristics of NF earthquakes. For the fling-step characteristics, a monotonic step is reflected in the displacement time history.
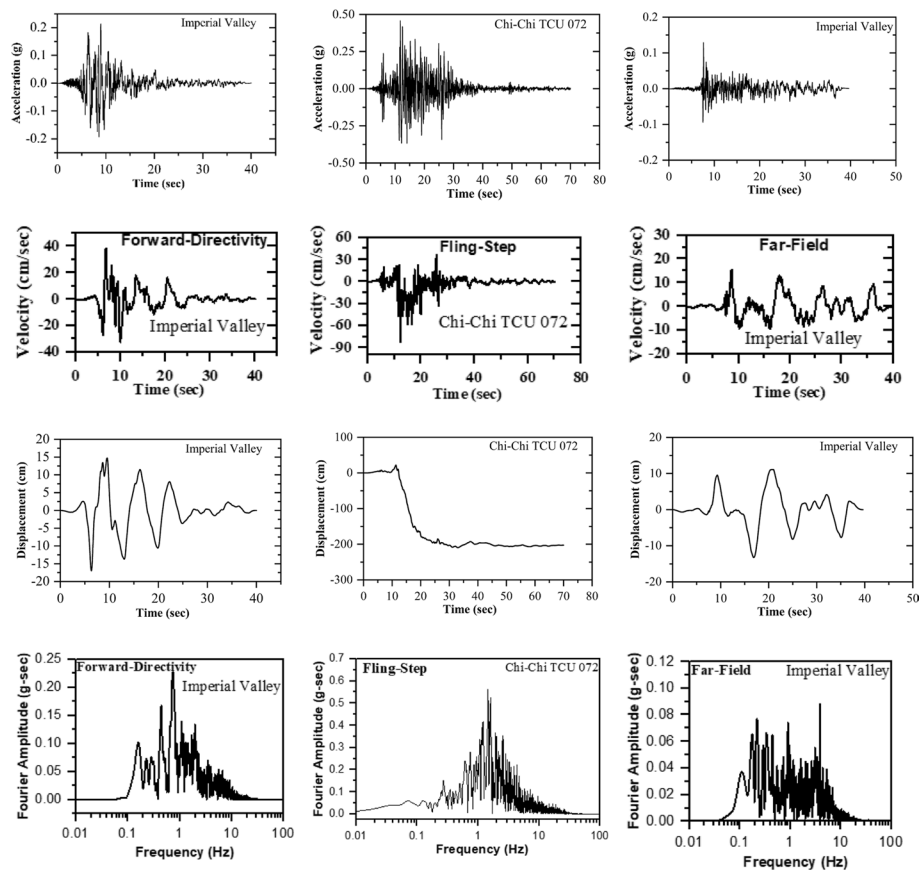

Fig. 1 Comparison of near-field forward directivity, fling step, and far-field earthquakes

Baig *et al. Journal of Engineering and Applied Science*   (2024) 71:115

Page 5 of 19

In summary, as depicted in Fig. 1, near-field (NF) records exhibit directivity and fling-step effects, resulting in peak amplitudes 1.5–2 times greater than nondirective signals, with dominant frequencies ranging from 20 to 100 Hz. In contrast, FF records, obtained from distant sources, do not display directivity effects and typically have dominant frequencies between 5 and 40 Hz. NF records show concentrated energy release, with pulse durations under 1 s, while FF records show dispersed energy from the seismic source, with longer durations ranging from 1 to 5 s [20]. Fling-step accelerograms, which exhibit high peak acceleration values, demonstrate an abrupt displacement in ground motion caused by energy release during seismic occurrences. These events produce a brief but intense shaking period due to the short duration of strong ground motion. The high-frequency content of the abrupt displacement can be observed by dominating frequencies between 5 and 100 Hz, which add to the severity of the seismic event and the sharpness of ground motion [25].

Modeling and design of lead rubber bearing

Rubber bearings made of steel plates for reinforcement and thin rubber layers bonded together. LRB employs rubber material, which possesses energy dissipation qualities, dampening features, and rubber's flexibility for seismic isolation [10]. The rubber utilized in LRB is a carefully designed composition that, when deformed, develops internal friction between the polymer and filler (such as carbon), allowing for the dissipation of energy as depicted in Fig. 2. The oval, rounded hysteresis curve of LRB is one of its distinguishing characteristics. It is usually highly helpful in reducing the high-mode vibration of superstructures, especially in significant deformation states. However, the stress-strain relationship's relative nonlinearity is caused by the polymer-filler structure's damping mechanism [3]. Therefore, applying the LRB in seismic isolation systems has often proven problematic for structural engineers due to the difficulties in numerically representing shear force displacement. The characteristics of the nonlinear restoring force have been accurately captured in a novel Bouc-Wen numerical model, which can be used with standard structure-design software. Because of this, simulating LRBs for practical applications is much simpler for structural engineers.

The parametric analysis aims to determine the optimal LRB isolation design parameters for a bridge under different ground motions, considering various isolator design parameters and ground motion features influencing earthquake-induced behavior. LRB isolators offer a significant lateral restorative capability, low horizontal and rotating stiffness, and high
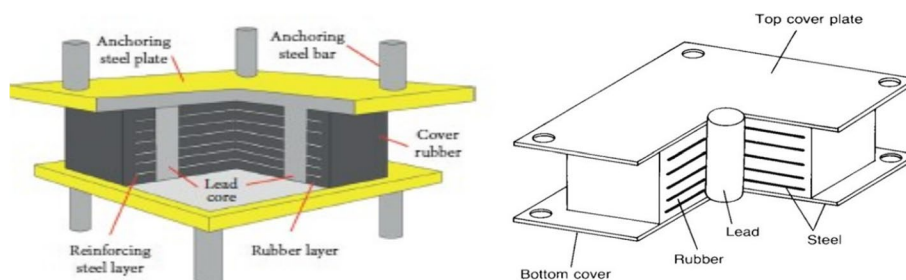

Fig. 2 Lead rubber isolators

vertical rigidity and bearing capacity. LRB has the most capability for dissipating energy due to lead core nearly perfect elastoplastic behavior under shear and its low yield strength [27].

The characteristic strength (Q), initial stiffness (Ku), effective damping, and post-yield stiffness (K_d) are the primary characteristics of the bilinear behavior of isolator that control the dissipation of energy. Other characteristics, in particular, post-yield stiffness (K_d) and yield strength (Fy), are either associated with the above two or have a significant impact. As a result, the primary characteristics of an isolator, Q and K_d, are highly correlated with the performance of bridge as measured by its effectiveness in decreasing the seismic demand. Typically, the characteristic strength plays a vital role in energy dissipation and damping, while the post-elastic rigidity significantly influences the regulation of horizontal flexibility and the isolation period as depicted in Fig. 3 [13]. The equations provided are used to compute important parameters of the hysteric curve of the isolators. The correlation between the isolator's characteristic strength (Q) and yield strength (Fy) is given by the following:

$$F_y = \frac{Q}{1 - \frac{K_d}{K_u}} \tag{1}$$

The characteristic strength (Q) is estimated by the area of the lead plug (A_p) and the shear yield stress of lead [11].

$$Q = f_{yp} \times A_p \tag{2}$$

$$Q = (K_u - K_d) \times D_y \tag{3}$$

$$\beta_{eff} = \frac{4 \times (D_{max} - D_y) \times Q}{2 \times \pi \times K_{eff} D^2} \tag{4}$$

$$K_d = \frac{G \times A_r}{H} \tag{5}$$

$$K_u = \frac{F_y}{D_y} \tag{6}$$

where G refers to the shear modulus of rubber, D_{max} is the design displacement of LRB, Ar is the area of rubber, H refers to total height of rubber in isolator, and Dy is the yield displacement of isolator.
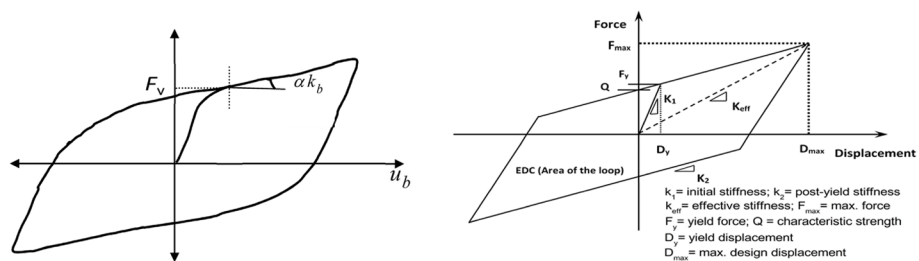

Fig. 3 Idealized hysteric curve for lead rubber isolator

Although it might be challenging to quantify, elastic stiffness (Ku) is typically assumed to be an empirical multiple of K_d [24]. This study uses the parameter of variations in characteristic strength (Q) normalized by the weight sustained on the LRB isolator, maintaining the superstructure characteristics constant while modifying the isolator's variables that significantly influence the bridge's response.

Methods

The numerical investigations are performed for a continuous steel box girder bridge in New Delhi, India, which is isolated by lead rubber (LRB) isolators. Three distinct LRB isolators are designed for various periods of isolation and strength to weight ratios (Q/W) to investigate their impact on bridges. The three protection levels that are represented by the wide range of isolation periods and effective stiffness that the proposed isolators cover are as follows:

Stiff isolators (Q/W = 0.12) with a high effective stiffness that leads the substructure to become inelastic.

Medium isolators (Q/W = 0.08) that retain the structure in an elastic state rather than an inelastic state. Flexible isolator (Q/W = 0.04) that maintains the substructure primarily in an elastic state, allowing for minimal inelastic effects.

The isolators are designed in accordance with the recommendations of Naeim and Datta for the entire dead load and 25% of the vehicle's load with a post-yield stiffness ratio of $\gamma = 0.10$ [6]. The fundamental time-period of the non-isolated bridge is 0.456 s. The study calculates effective stiffnesses for three isolators based on assumed time periods and design parameters, with the aim of demonstrating the differences in behaviors for different flexible isolations. The nonlinear direct integration time history analyses are performed in the longitudinal direction of the bridge. Table 1 lists the key properties of isolation devices used for bilinear modeling of isolator for the three developed isolators: flexible, medium, and stiff.

Table 1 Properties of isolation devices used for bilinear modeling

Q/W	Time period	Effective stiffness	Post-yield stiffness	Characteristic strength	Eff. damping	Yield strength	Design disp.
	s	K_{eff} (KN/m)	K_2 (KN/m)	Q (KN)	β_{eff}	F_y (KN)	Dmax. mm
Bent							
0.04 (flexible)	2.5	1567.2	1045	104.5	0.15	116.1	195
0.08 (medium)	1.85	3134.5	2089.6	209	0.21	232.1	140
0.12 (stiff)	1.5	4701.6	3134.5	313	0.29	348.2	115
Abutment							
0.04 (flexible)	2.5	487.8	325.2	32.5	0.15	36.13	195
0.08 (medium)	1.85	975.6	650.4	65.1	0.21	72.2	140
0.12 (stiff)	1.5	1464	976	97.5	0.29	108.4	115

Six NF and two FF earthquake records are obtained from the PEER database for the numerical study. Four of the six NF records have directivity effects, while the other two have fling-step effects. The selected earthquake records have been scaled to three PGA levels of 0.2 g, 0.4 g, and 0.8 g after being normalized in accordance with FEMA. According to FEMA regulations, ground motion is normalized by its matching peak spectral velocity to reduce undesired variance in the recordings caused by variations in source type, site condition, event size, and distance to source. The ratio of the highest recorded velocity to the median peak spectral velocity is used as the earthquake's normalizing factor. The acceleration time histories of the ground motion are then multiplied by the normalized factors [12].

This study attempts to investigate the inadequate accurate ground motion records in New Delhi, India, by comparing acceleration time histories from other parts of the world with similar fault systems, site features, and seismic potential. Table 2 lists the significant features of the records.

Finite element modeling of bridge

The study focuses on a steel box girder continuous bridge having reinforced circular concrete piers [4]. The bridge is 147.88 m long overall, with spans of 27.5, 34.2, 36.5, and 29.4 m, as depicted in Fig. 4. Two continuous steel box girder deck systems and a top slab measuring 10 m in width compose the superstructure. The depth of girder is 1.545 m, and the effective slab thickness is 300 mm. The bents are made up of a double circular reinforced concrete pier supported by a tapering rectangular cross section cap beam. The 1.6-m diameter and 7.6-m height bents reinforced concrete pier is supported up by pile footings. Each pier comprises 10-mm spiral hoops spaced 150 mm apart and 32 vertical bars with a diameter of 32 mm. While the characteristic strength of reinforcing steel is HYSD 415, the unconfined compressive characteristic strength of concrete is M40 in the deck and M45 in the pier. The girder, which remains elastic during seismic excitations, is represented by the elastic beam-column element. The section determines characteristic quantities like cross-sectional area, torsional moment of inertia, and second moments of area, and the element mass per unit length is used for dynamic analysis [9].

Table 2 Selected earthquake records

Earthquake	Year	M_w	Station	PGA (g)	Rjb (km)	PGV (cm/s)	PGV/PGA
Near-field forward directivity (high frequency)							
Imperial Valley	1979	6.54	County center	0.21	7.31	38.40	181.13
Kobe Japan	1995	6.9	Takatori	0.62	1.46	121.00	195.79
Near-field forward directivity (low frequency)							
Imperial Valley	1979	6.53	Agrarias	0.29	0.1	33.8	116.5
Kobe Japan	1995	6.9	KJMA	0.83	0.94	91.10	109.76
Near-field fling step							
Chi-Chi	1999	7.6	TCU 072	0.46	7.90	82.50	180.53
Chi-Chi	1999	7.6	TCU 075	0.32	3.40	111.70	349.06
Far field							
Imperial Valley	1979	6.54	Idel station	0.13	24.2	16.8	129.2
Kobe, Japan	1995	6.9	MZH	0.068	69.04	5.17	76.0

Baig *et al. Journal of Engineering and Applied Science*   (2024) 71:115
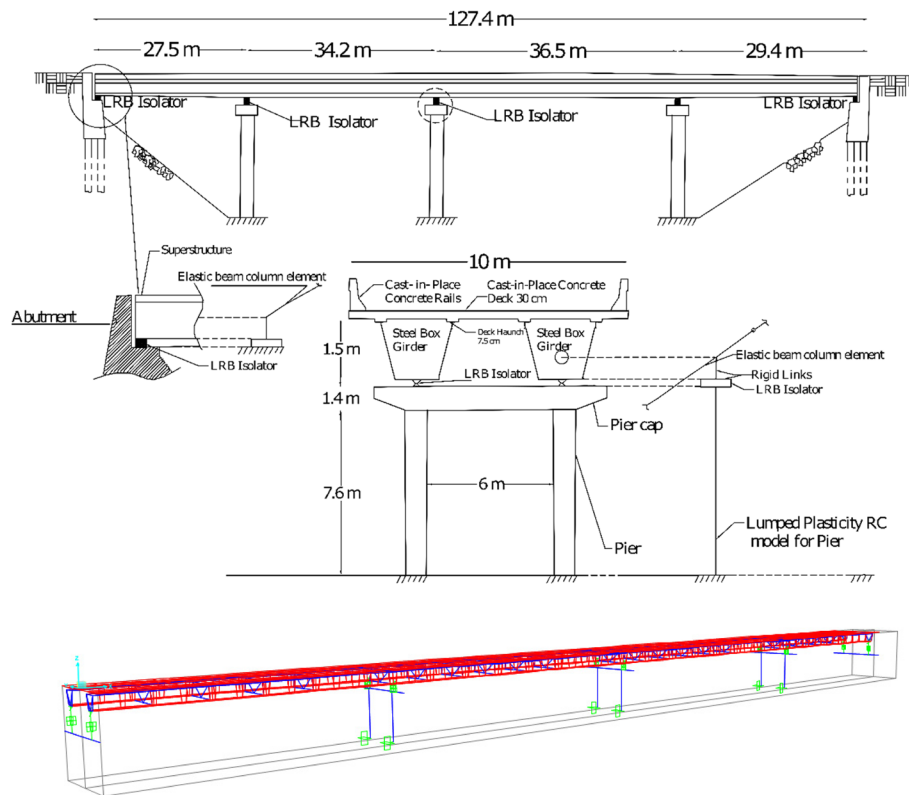
Page 9 of 19

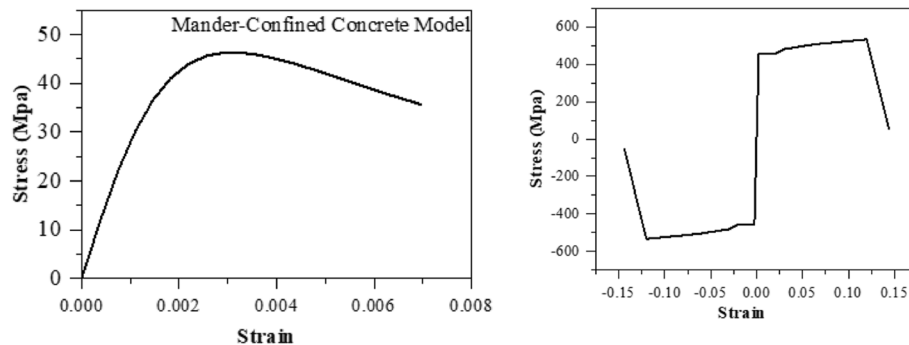**Fig. 4** Detail of steel box girder bridge and FEM model

Fig. 5 Concrete and steel material model

Due to the anticipated inelastic excursions of piers and the protection offered by a capacity design, the deck's superstructure, which consists of elastic beam-column elements made of cracked reinforced concrete, is not considered as nonlinear in a bridge assessment [8]. In the present study, confined and unconfined concrete are simulated using the Mander concrete model from CSI Bridge, as depicted in Fig. 5. Pier plastic hinges are simulated using the interaction PMM hinge model, which predicts pier post-yield behavior. Real and idealized M-ϕ must be balanced in order to generate the idealized moment-curvature curve. The steel material model exhibiting symmetrical compression and tension behavior predicts a yield plateau and strain hardening zone that arise from

Baig *et al. Journal of Engineering and Applied Science*   (2024) 71:115

Page 10 of 19

an initial elastic state up to yield. At the pier's point of fixity, plastic hinges are developed [5]. The connections between the substructures and superstructures are among the most crucial structural elements of the bridge. Two LRB isolator systems are placed on pier caps and abutments to support superstructure deformations during seismic events. Under shear stresses, LRB behavior is a bilinear model with typical properties like initial stiffness, stiffness at post-yield state, and yield strength. While for non-isolated bridge, the bents are supported by steel rocker bearings and the abutments by steel roller bearings. The study does not consider soil structural interaction and abutment stiffness in the dynamic analysis of the bridge due to the focus on comparing responses, considering a stiff site condition, and for convenience of analysis. The Bouc-Wen model is utilized to simulate the LRB isolator and the force-deformation curve [19]. The finite element program CSI Bridge is used for numerical modeling, with the stiffness at the end of the nonlinear load case used for direct integration dynamic analysis. The superstructure dead load and superimposed dead loads from the crash barrier, wearing coat, and footpath slab are included in the nonlinear load case. For the first and second modes of vibration, 5% Rayleigh damping was used.

Results and discussion

The present investigation assessed the dynamic characteristics and seismic response of isolated steel box girder bridge with different mechanical properties of LRBs, such as characteristic strength to weight sustained by isolators (Q/W) and isolation period. The performance of the isolated bridge under the (i) NFD-HF, (ii) NFD-LF, (iii) NF-FS, and (iv) FF ground motions is compared for various damage measures such as maximum pier displacement (MPD), base shear (MBS), deck acceleration (MDA), and hysteretic curve dissipated energy (HED). Responses are extensively investigated within the three seismically expected levels, namely design level (0.2 g), extreme level (0.4 g), and rare-extreme level (0.8 g), in order to explore the response of the isolated bridge. In the following subsections, the response of a specific isolated steel box girder bridge under various earthquakes is discussed.

Pier displacement

The top pier displacement (MPD) of isolated bridges with specified Q/W ratios and isolation period is computed under the selected ground motions at three various PGA levels. Fig. 6 also depicts the variation of the MPD at the rare-extreme level of PGA. Fig. 7 shows that the bridges supported by LRBs with different isolation parameters successfully reduced MPD demand, notably under flexible and medium isolators. Although the response of MPD under different earthquakes considering the stiff isolators are significant. When compared to non-isolated bridge, the response of the MPD to different earthquakes is considerably decreased, demonstrating the efficacy of the LRB isolator.

From Fig. 7, it can be inferred that increasing the Q/W ratios seems to result in higher pier displacements. In the case of the NFD-HF earthquake, for instance, the stiff isolator led to 2.68 times greater pier displacement than the flexible isolator at the rare-extreme level of PGA.

It is observed from Table 3 that ground motion with high PGV/PGA ratios has a large MPD, whereas those with low PGV/PGA ratios have relatively low MPD. High
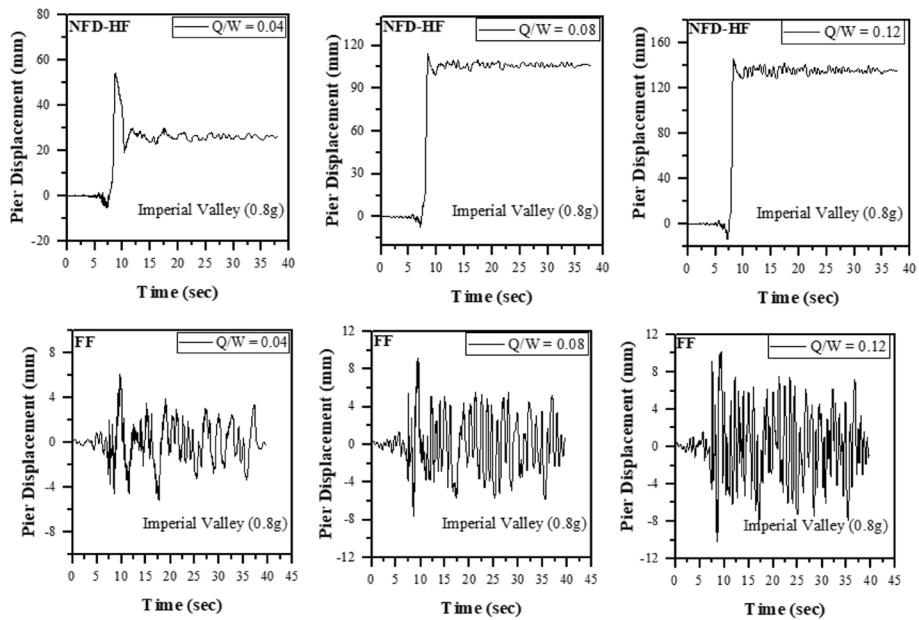
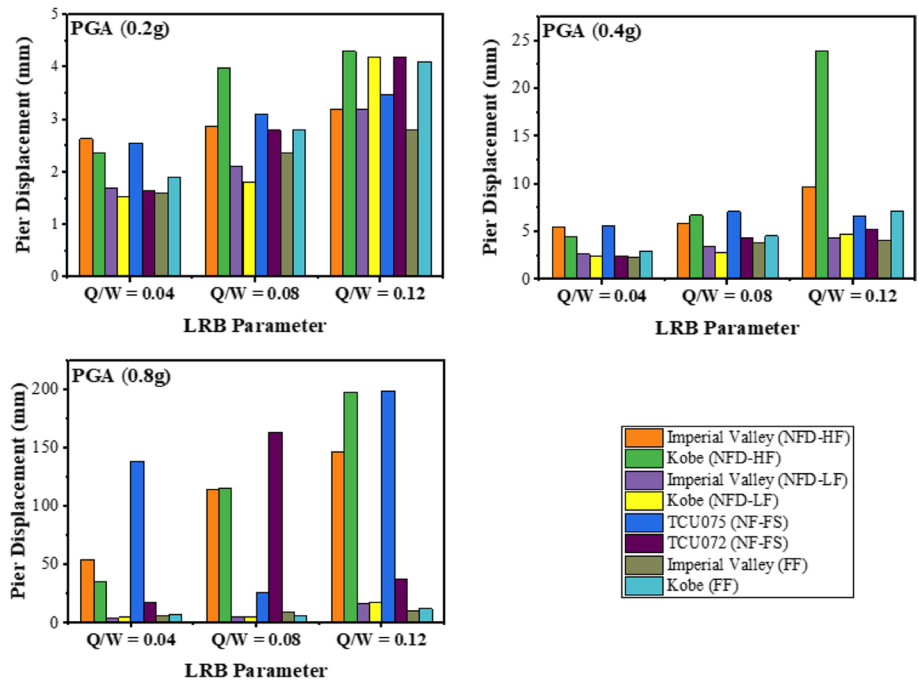**Fig. 6** Time history plots for top pier displacement

Fig. 7 Comparison of pier displacement at different strength ratios

PGV/PGA ratios are often linked to moderate to severe earthquakes with high frequency contents and irregular acceleration pulses, which rapidly load and unload the isolated bridge.

Baig *et al. Journal of Engineering and Applied Science*   (2024) 71:115

Page 12 of 19

Table 3 Maximum pier top displacement for various Q/W ratios of LRB

| Earthquake	Pier top displacement (mm)											
	Non-isolated			LRB (Q/W) = 0.04			LRB (Q/W) = 0.08			LRB (Q/W) = 0.12		
	0.2 g	0.4 g	0.8 g	0.2 g	0.4 g	0.8 g	0.2 g	0.4 g	0.8 g	0.2 g	0.4 g	0.8 g
NFD-HF												
Imperial Valley	28	57.8	307	2.63	5.5	54.5	2.8	5.9	114.1	3.2	5.7	146.1
Kobe	26	97	398	2.37	4.5	35.1	3.9	6.8	115.4	4.3	23.9	197.4
NFD-LF												
Imperial Valley	15.9	61	223	1.6	2.7	4.6	2.1	3.47	5.4	3.2	4.4	16.2
Kobe	20.9	63.6	217	1.5	2.4	4.8	1.8	2.88	4.9	4.2	5.7	18.1
NF-FS												
Chi-Chi (TCU072)	22.1	46.7	124.8	1.65	2.4	17.4	2.8	4.4	25.8	4.1	5.3	37.2
Chi-Chi (TCU075)	26.6	54.2	234	2.55	5.6	138.6	3.1	7.1	163.5	3.4	6.7	198.4
FF												
Imperial Valley	8.9	18.5	57.9	1.6	2.4	6.1	2.3	3.9	9.2	2.8	4.1	10.2
Kobe	20.2	37.9	106.1	1.9	2.9	7.3	2.8	4.6	9.4	4.1	7.2	12.4
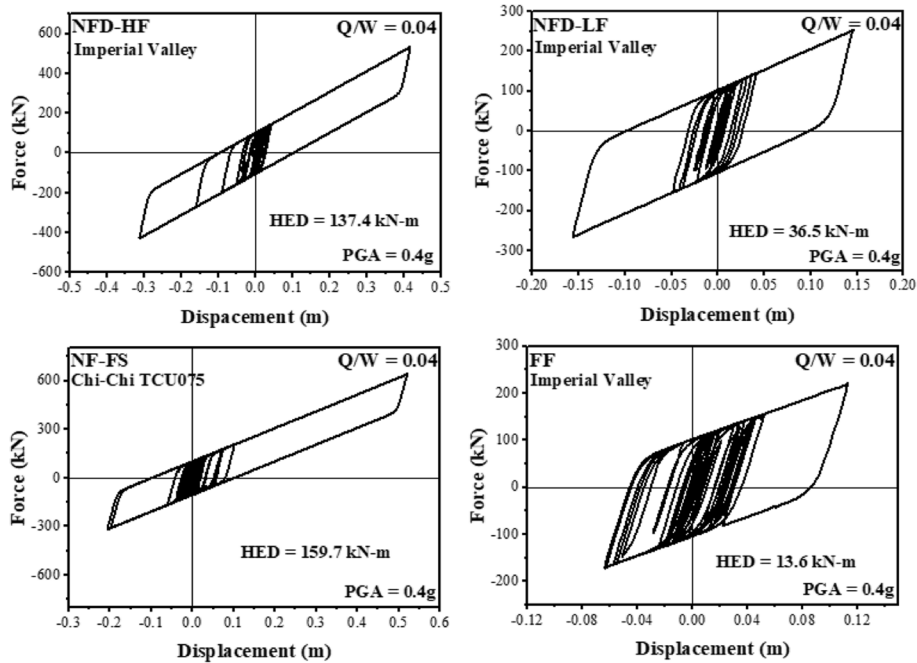
Fig. 8 Isolator force-deformation curve at PGA of 0.4 g for Q/W = 0.04 under NF and FF earthquakes

Hysteresis energy dissipation

The hysteretic curves for the isolation systems and bent pier exposed to different earthquakes are depicted in Figs. 8, 9 and 10 while accounting for varied Q/W ratios and isolation periods. Maximum energy dissipation is depicted in Fig. 8 by a lower Q/W ratio and a longer isolation period. Since flexible isolators are less stiff than conventional isolation systems, they provided horizontal flexibility. Fig. 9 reveals varying force displacement behavior of isolators across earthquake types and PGA levels, with cycles of isolator displacement occurring in the center zone at close intervals. At the larger PGA
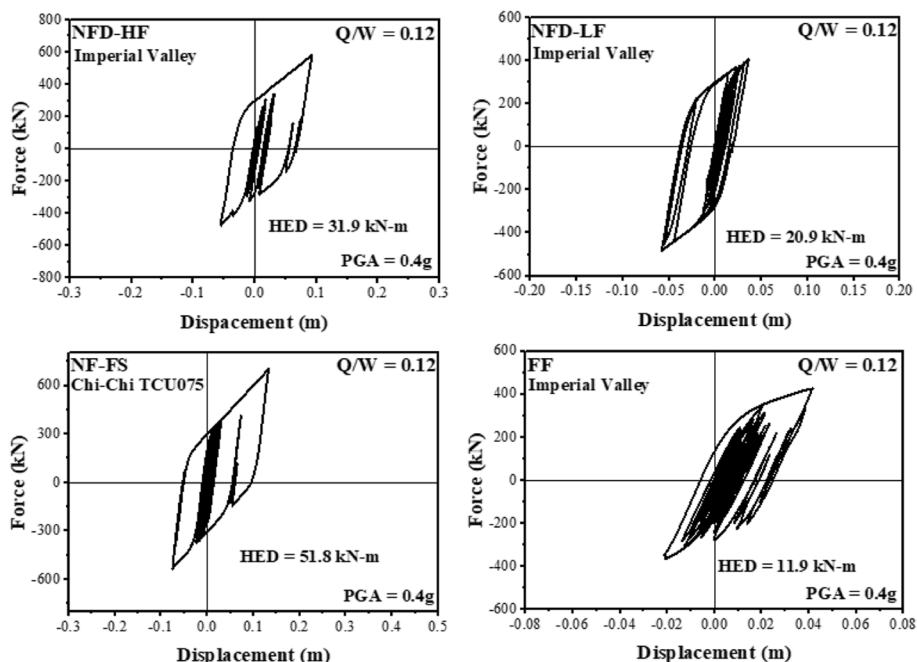
Fig. 9 Isolator force-deformation curve at PGA of 0.4 g for Q/W = 0.12 under NF and FF earthquakes

levels, the area of hysteresis loop expands. At design level of PGA, the isolator's hysteretic energy dissipation (HED) is 137.4 kN-m for NFD-HF, 36.5 kN-m for NFD-LF, 159.7 kN-m for NF-FS, and 13.6 kN-m for FF earthquakes, respectively for low Q/W ratio. Fig. 10 depicts an increased Q/W ratio indicates that the structural response is primarily influenced by the stiffness of the supporting bent pier. As seismic forces are applied to the structure, most energy is absorbed and dissipated within the supporting pier, which undergo deformation mechanisms, leading to increased energy dissipation. Therefore, a large Q/W ratio reduces energy dissipation within the isolator due to its stiffness while increasing energy dissipation within the supporting pier.

Observations reveal that at the identical PGA level, the value of HED is considerably higher in the event of NFD-HF and NF-FS earthquakes than to NFD-LF and FF earthquakes.

Table 4 depicts the amount of hysteresis energy that each isolation system and bent pier dissipated under various earthquake conditions. It is evident that decreasing the isolation period and increasing the Q/W ratio resulted in a reduction in the excessive isolator displacement demand. Ultimately, by selecting the appropriate isolation parameters of LRB, namely the Q/W ratio and isolation period, the efficacy of the isolation systems can be controlled.

Base shear

The influence of a predefined Q/W ratios on MBS for the NFD-HF, NFD-LF, NF-FS, and FF earthquakes at three PGA levels is presented in Fig. 11. It is evident from Fig. 12 that the increase in Q/W ratio leads to increase in the base shear. This increase is more noticeable under NFD-HF and NF-FS ground motions. A considerable change in base
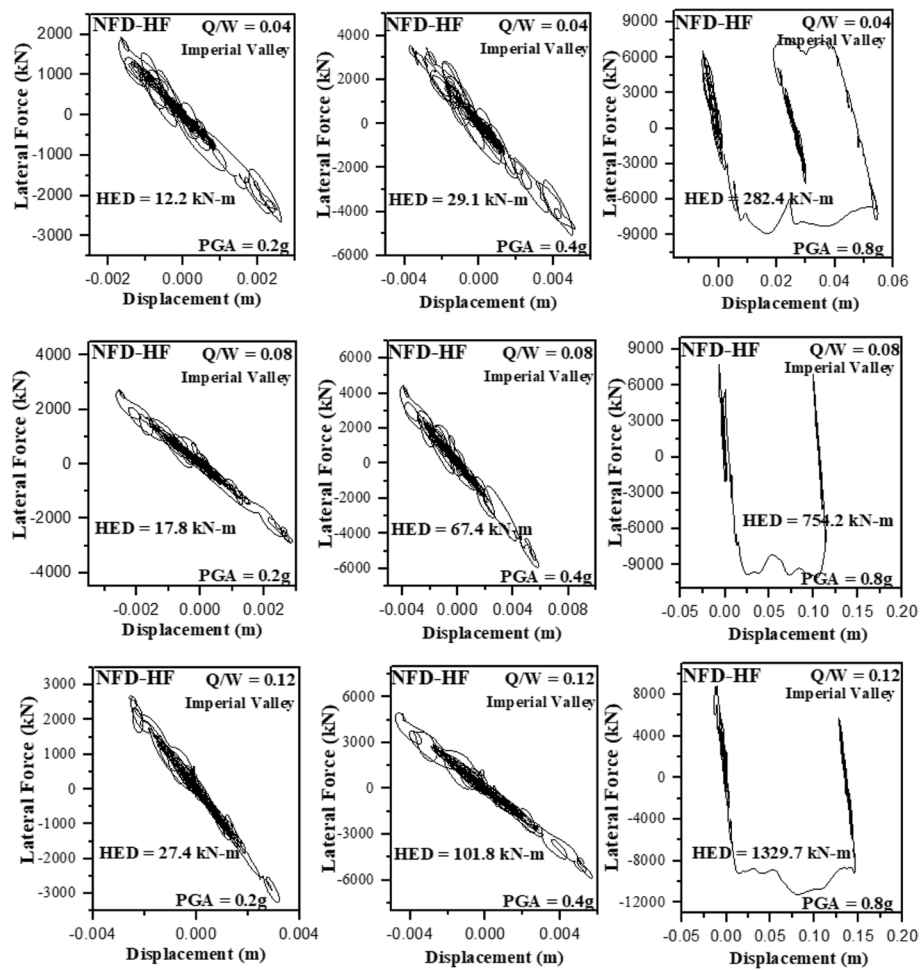
Fig. 10 Comparison of hysteric energy dissipation of bent pier at different isolator's strength ratios and PGA levels

shear is observed due to variation in Q/W ratios. It is due to the large displacement under NF earthquakes even at low PGA level.

In addition, from the change in Q/W ratios from 0.12 to 0.04, varying the isolation period from 1.5 to 2.5 s resulted in a consistent reduction in base shear, depicted in Fig. 12. The higher PGA levels, 0.4 g and 0.8 g, do not exhibit a consistent pattern. At high PGA levels in NFD-HF and NF-FS ground motions, the inelastic excursion occurs in the bridge, and that indicates the base shear fails to show any consistency due to the complexity of seismic energy dissipation in the bridge. It is observed that the base shear initially decreases to the lowest value and then increases as the Q/W ratio increases. This suggests that there is a particular level of Q/W ratio for which the base shear is at its lowest.

Deck acceleration

The maximum absolute accelerations under various earthquakes with yield strength ratio and isolation period are presented in Fig. 13. It was observed that reduction of the yield strength ratio remarkably caused to mitigate the maximum absolute acceleration

Table 4 Hysteric energy dissipation for different isolator's strength ratios

| Earthquake		Hysteric energy dissipation (KN-m)								
		LRB (Q/W) = 0.04			LRB (Q/W) = 0.08			LRB (Q/W) = 0.12		
		0.2 g	0.4 g	0.8 g	0.2 g	0.4 g	0.8 g	0.2 g	0.4 g	0.8 g
NFD-HF										
Imperial Valley	LRB isolator	19.1	137.4	794.8	9.75	57.2	338.5	5.18	31.9	194.8
	Bent pier	12.2	29.1	282.4	17.8	67.4	754.2	27.4	101.8	1329.7
Kobe	LRB isolator	37.4	193.2	923.6	33.1	180.2	697.2	26.3	97.8	561.4
	Bent pier	26.6	44.3	412.4	43.3	116.4	1330	62.4	398.3	2456.7
NFD-LF										
Imperial Valley	LRB isolator	9.65	36.5	143.2	7.75	31.5	103.7	7.78	20.9	82.7
	Bent pier	4.6	13.2	68.4	7.3	48.4	162.3	18.7	92.4	321.4
Kobe	LRB isolator	5.2	29.8	98.4	6.21	24.7	82.8	5.6	13.78	61.3
	Bent pier	3.8	19.4	63.6	8.81	86.2	271.7	6.4	127.9	486.4
NF-FS										
Chi-Chi (TCU072)	LRB isolator	7.1	22.7	80.3	5.6	14.8	68.9	4.98	12.7	58.6
	Bent pier	5.2	13.6	64.8	9.6	63.4	212.3	19.6	87.3	416.2
Chi-Chi (TCU075)	LRB isolator	20.7	159.7	824.4	11.77	67.7	404.5	10.1	51.8	256.8
	Bent pier	19.7	216.3	444.6	22.6	86.3	856.4	76.2	119.3	1544.6
FF										
Imperial Valley	LRB isolator	4.8	13.6	81.8	4.06	10.8	49.2	4.35	11.9	41.45
	Bent pier	2.2	6.4	44.6	2.9	7.4	84.4	9.84	76.6	287.4
Kobe	LRB isolator	4.72	11.6	70.7	3.92	9.42	38.6	3.81	10.1	33.2
	Bent pier	2.9	8.8	52.4	5.3	19.7	94.7	12.7	98.4	326.7
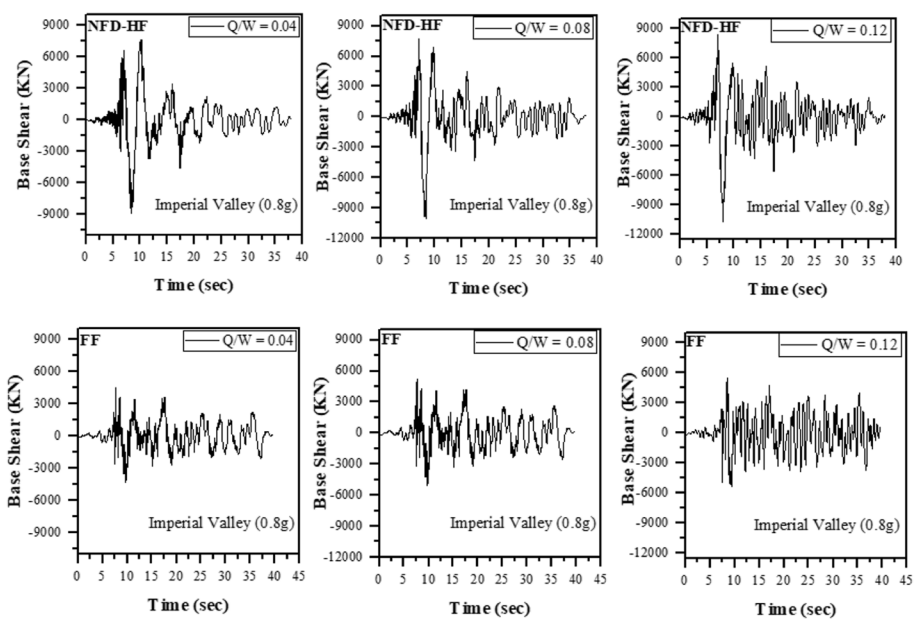
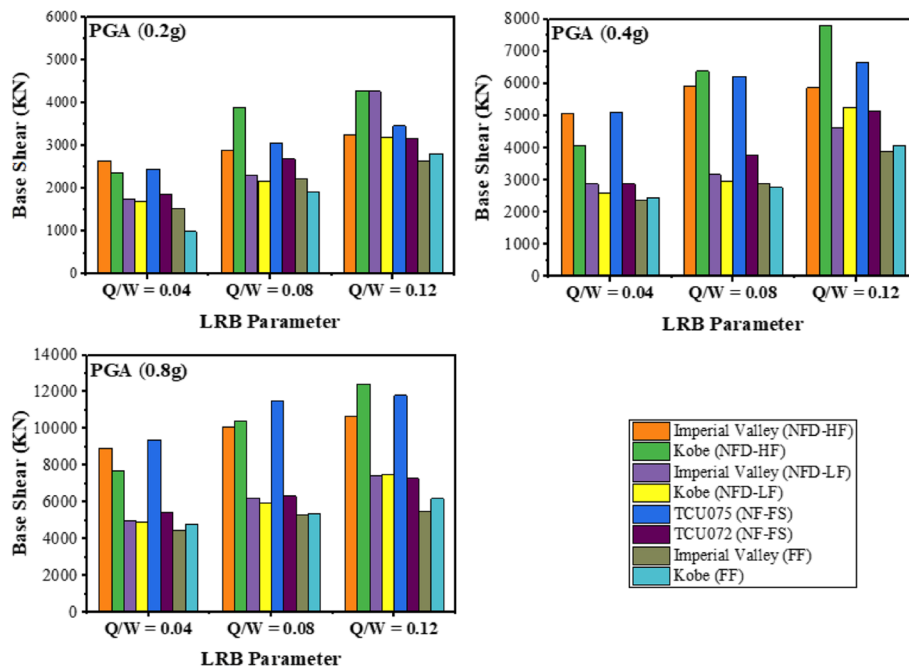**Fig. 11** Comparison for base shear at different isolator's strength ratios

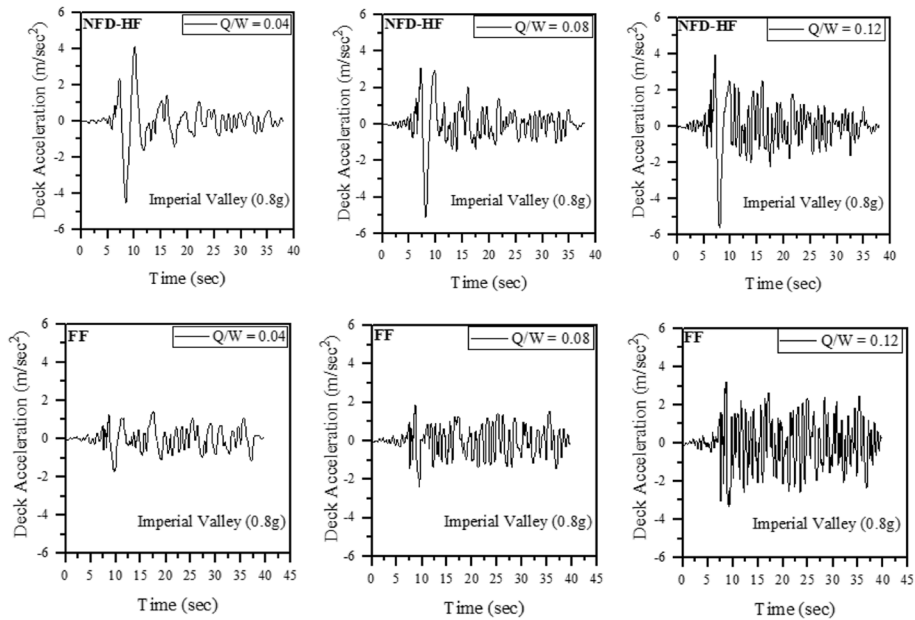**Fig. 12** Time history plots for base shear under NF and FF earthquakes

Fig. 13 Time history plots for maximum deck acceleration under NF and FF earthquakes

except the inefficient performance of under the Kobe and Chi-Chi earthquake seismic isolation was found generally effective in mitigating deck accelerations. As compared to non-isolated bridge, the deck acceleration is successfully reduced at lower yield strength ratios. Furthermore, when the Q/W ratio rises, the deck acceleration first falls to the minimal value and then rises.

Table 5 shows the maximum absolute accelerations under different earthquakes as a function of yield strength ratio and isolation time. Except for the poor performance of seismic isolation under the Kobe and Chi-Chi earthquakes, it was found that lowering the yield strength ratio significantly reduced the highest absolute acceleration. Deck acceleration is effectively decreased at lower yield strength ratios when compared to a non-isolated bridge. However, as the Q/W ratio rises, the deck acceleration reduces initially and then increases.

Conclusions

The study examines the analytical seismic response of a seismically isolated bridge using various ground motion and isolation parameters. The results are analyzed using pier displacement, deck displacement, deck acceleration, base shear, and isolator hysteric energy dissipation. Smaller MPD, MDA, MBS, and HED values for a given ground motion indicate better seismic performance. Identifying ideal values for Q/W, isolation period, and post-yield stiffness ratio is challenging due to various design parameters. However, adequate ranges of Q/W ratios, isolation period, and post-yield stiffness ratio can be recommended for the early design of seismically isolated bridges using LRB isolators. High PGV/PGA ratio ground motions possess a major impact on the bridge's performance, whereas low PGV/PGA ratio has less influence. High PGV/PGA ratios are often linked to moderate to severe earthquakes with high frequency and irregular acceleration pulses, which rapidly load and unload the bridge. The following conclusions and suggestions are made based on the findings of the analyses:

- The pier displacement, base shear, and deck acceleration demand were successfully decreased by the bridges supported by LRBs with varying isolation parameters, especially under flexible and medium isolators. However, the response under stiff isolators is not particularly significant.
- The characteristics of the earthquakes, in addition to the Q/W ratio, had a significant impact on the variation in response. For instance, in comparison to NFD-LF

Table 5 Maximum deck acceleration for different isolator's strength ratios

Earthquake	Non-isolated			LRB (Q/W) = 0.04			LRB (Q/W) = 0.08			LRB (Q/W) = 0.12		
	0.2 g	0.4 g	0.8 g	0.2 g	0.4 g	0.8 g	0.2 g	0.4 g	0.8 g	0.2 g	0.4 g	0.8 g
NFD-HF												
Imperial Valley	2.86	3.44	5.88	1.12	2.2	4.5	1.24	2.58	5.13	1.35	2.75	5.6
Kobe	3.37	3.78	6.1	1.25	2.4	4.91	1.85	3.4	5.88	2.1	3.84	6.9
NFD-LF												
Imperial Valley	2.86	3.44	3.94	0.72	1.17	2.16	0.93	1.28	2.76	1.50	2.12	3.85
Kobe	3.37	3.78	4.68	0.74	1.24	2.15	0.98	1.57	2.92	2.1	2.48	4.12
NF-FS												
Chi-Chi (TCU072)	3.2	3.49	4.27	0.75	1.19	2.04	1.32	1.82	2.72	1.9	2.66	3.95
Chi-Chi (TCU075)	3.45	4.28	6.1	1.29	2.68	4.45	1.40	3.12	5.94	1.52	3.93	6.78
FF												
Imperial Valley	1.96	3.32	3.64	0.6	0.95	1.73	1.1	1.24	2.36	1.34	1.83	3.32
Kobe	1.68	3.02	3.57	0.48	0.68	0.96	1.02	1.23	1.58	1.62	1.97	2.97

Baig *et al. Journal of Engineering and Applied Science*   (2024) 71:115

Page 18 of 19

and FF, the response of the bridge to NFD-HF and NF-FS ground motions is significantly higher.

- As the Q/W ratios rise, the MPD increases, while the MID declines. The decrease in the MID is due to the fact that as the Q/W ratio increases, the separation system becomes more rigid, and thus, the bearing displacements decrease. Although the base shear and deck acceleration decrease first, eventually reaching a minimum, and subsequently increase as the Q/W ratio increases.
- For bridge structures situated at locations with high PGV/PGA records, isolators with a low Q/W ratio can be used to reduce forces transmitted to the substructures while keeping MIDs within an acceptable range.
- It is observed that a reduction in Q/W ratio remarkably reduces the maximum absolute acceleration, except for the inefficient performance under the Kobe and Chi-Chi (TCU075) earthquake.
- The hysteric loop of an isolator significantly impacts the type of earthquake. Near-field earthquakes have fewer loops and elongated hysteresis loops, causing significant isolator displacement, especially at higher PGA levels. Far-field earthquakes have more hysteresis cycles, resulting in less displacement.
- A high Q/W ratio results in decreased dissipation of energy within the isolator, while it leads to increased dissipation of energy within the supporting columns.
- In comparison to FF earthquakes, the isolation system dissipates large amount of hysteretic energy under the influence of NFD-HF and NF-FS earthquakes.

Abbreviations

NF	Near Field
FF	Far Field
LRB	Lead rubber bearing
FPS	Friction pendulum system
NFD-HF	Near-field forward directivity
NF-FS	Near-field fling step
PGA	Peak ground acceleration
PGV	Peak ground velocity
MPD	Maximum pier displacement
MBS	Maximum base shear
HED	Hysteretic energy dissipation
Q	Characteristic strength of LRB
W	Weight sustained by LRB isolator
Ku	Initial stiffness
Kd	Post-yield stiffness
Fy	Yield strength
β_{eff}	Effective damping

Authors' contributions
All authors have participated in the work through, prepared the data and modeling, carried out the program, analyzed the results, wrote the manuscript, and approved the final draft.

Availability of data and materials
Data can be shared upon request.

Declarations

References

1. Afreen A, Ahmed A and Moin K. (2021) Effect of near-field earthquake on masonry structure. Asian J Civil Eng, (0123456789). https://doi.org/10.1007/s42107-021-00353-4
2. Asadi P, Nikfar D, Hajirasouliha I (2020) 'Life-cycle cost based design of bridge lead-rubber isolators in seismic regions.' Structures 27(December 2019):383–395. https://doi.org/10.1016/j.istruc.2020.05.056
3. Baig MA et al (2022) Effect of lead rubber bearing on seismic performance of steel box girder bridge. Mater Today 64:468–480. https://doi.org/10.1016/j.matpr.2022.04.953
4. Baig, M. A. et al. (2023). Vulnerability assessment of steel box-girder bridge under near-field and far-field earthquakes. Innov Infrastructure Solutions, 8(1). https://doi.org/10.1007/s41062-022-00983-w
5. Berry MP, Eberhard MO (2005) Practical performance model for bar buckling. J Struct Eng 131(7):1060–1070. https://doi.org/10.1061/(asce)0733-9445(2005)131:7(1060)
6. Bhandari M et al (2018) The numerical study of base-isolated buildings under near-field and far-field earthquakes. J Earthquake Eng 22(6):989–1007. https://doi.org/10.1080/13632469.2016.1269698
7. Bhandari M et al (2019) Seismic fragility analysis of base-isolated building frames excited by near- and far-field earthquakes. J Perform Construct Facilities 33(3):04019029. https://doi.org/10.1061/(asce)cf.1943-5509.0001298
8. Bhuiyan, A. R., Alam, R. and Haque, N. (2012) 'Seismic performance assessment of a continuous highway bridge seismically isolated by lead rubber bearings', 02(03), pp. 62–71
9. Billah AHMM, Alam MS, Bhuiyan MAR (2013) Fragility analysis of retrofitted multicolumn bridge bent subjected to near-fault and far-field ground motion. J Bridge Engin 18(10):992–1004. https://doi.org/10.1061/(asce)be.1943-5592.0000452
10. Chen L, Jiang L, Liu P (2011) Dynamic properties of lead rubber bearings and its seismic isolation applications in high-speed railway bridge. Adv Mater Res 150–151:164–167. https://doi.org/10.4028/www.scientific.net/AMR.150-151.164
11. F. Naeim and J. M. Kelly (1999) 'Design of seismic isolated structures: from theory to practice', Earthquake Spectra, 16(3). Available at: http://earthquakespectra.org/doi/abs/10.1193/1.1586135
12. Federal Emergency Management Agency (2020) 'Hazus Earthquake Model Technical Manual ', Federal Emergency Management Agency, (October), pp. 1–436
13. Hameed A et al (2008) Effect of lead rubber bearing characteristics on the response of seismic-isolated bridges. KSCE J Civil Eng 12(3):187–196. https://doi.org/10.1007/s12205-008-0187-9
14. Hassan AL, Billah AM (2020) Influence of ground motion duration and isolation bearings on the seismic response of base-isolated bridges. Eng Struct 222(June):111129. https://doi.org/10.1016/j.engstruct.2020.111129
15. Kunde MC, Jangid RS (2006) Effects of pier and deck flexibility on the seismic response of isolated bridges. J Bridge Eng 11(1):109–121. https://doi.org/10.1061/(asce)1084-0702(2006)11:1(109)
16. Lin Y et al (2021) Across-fault ground motions and their effects on some bridges in the 1999 Chi-Chi earthquake. Adv Bridge Eng 2(1):1–21. https://doi.org/10.1186/s43251-020-00028-1
17. Losanno D, Hadad HA, Serino G (2017) Seismic behavior of isolated bridges with additional damping under far-field and near fault ground motion. Earthquake Struct 13(2):119–130. https://doi.org/10.12989/eas.2017.13.2.119
18. Miano A et al (2024) Seismic fragility of circular piers in simply supported RC bridges: a proposal for capacity assessment. Eng Struct 302(December 2023):117426. https://doi.org/10.1016/j.engstruct.2023.117426
19. Mitoulis SA, Rodriguez Rodriguez J (2017) Seismic performance of novel resilient hinges for columns and application on irregular bridges. J Bridge Eng 22(2):1–12. https://doi.org/10.1061/(ASCE)BE.1943-5592.0000980
20. Mukhopadhyay S, Gupta VK (2013) Directivity pulses in near-fault ground motions-I: identification, extraction and modeling. Soil Dynamics Earthquake Eng 50:1–15. https://doi.org/10.1016/j.soildyn.2013.02.017
21. Shahbazi S. et al. (2019) Seismic response of steel smfs subjected to vertical components of far-and near-field earthquakes with forward directivity effects. Adv Civil Eng. 2019. https://doi.org/10.1155/2019/2647387
22. Sharma V et al (2021) Seismic fragility evaluation of semi-rigid frames subjected to near-field earthquakes. J Construct Steel Res 176:106384. https://doi.org/10.1016/j.jcsr.2020.106384
23. Somerville, P. G. (2002) 'Characterizing near fault ground motion for the design and evaluation of bridges', Proceedings 3rd National Seismic Conference & Work shop on Bridges & Highways, Portland, Oregon, (01), pp. 137–148
24. Vibhute AS et al (2022) Performance evaluation of FPS and LRB isolated frames under main and aftershocks of an earthquake. Structures 44(August):1532–1545. https://doi.org/10.1016/j.istruc.2022.08.082
25. Yadav KK, Gupta VK (2017) 'Near-fault fling-step ground motions: characteristics and simulation.' Soil Dynamics Earthquake Eng 101(December 2015):90–104. https://doi.org/10.1016/j.soildyn.2017.06.022
26. Yang, J. et al. (2021) 'Near-fault ground motion influence on the seismic responses of a structure with viscous dampers considering SSI effect. Adv Civil Eng. 2021. https://doi.org/10.1155/2021/6649124
27. Zheng W. et al. (2020) 'Performance of bridges isolated with sliding-lead rubber bearings subjected to near-fault earthquakes. Int J Struct Stabil Dynamics. 20(2). https://doi.org/10.1142/S0219455420500236
28. Zhou T, Li AQ (2020) Stochastic modeling and synthesis of near-fault forward-directivity ground motions. KSCE J Civil Eng 24(2):483–498. https://doi.org/10.1007/s12205-020-0390-x